Robust and Fast Medical Registration of 3D-Multi-Modality Data Sets

M. Čapek, L. Mroz and R. Wegenkittl*

VRVis Center, Lothringerstraße 16/4, A-1030 Vienna, Austria, *www.vrvis.at*, contact address: *capek@vrvis.at*
*TIANI Medgraph GmbH, Campus 21, Liebermannstraße A01 303, A-2345 Brunn am Gebirge, Austria, *www.tiani.com*

Abstract
A fully-automatic approach to volume registration based on global information content is described. In a nutshell this task represents an optimization problem that has been solved with respect to robustness and computational speed especially. Strong attention has been paid to the choice of an optimized function that measure the quality of the registration (Mutual Information), to the choice of an optimization strategy that searches for a global optimum of the function in a parametric space (Adaptive Simulated Annealing), and to the efficient way of registration procedure implementation that includes region-of-interest segmentation, multi-resolution strategy and an incremental approach to volume resampling.

1. Introduction

Nowadays, patients are frequently investigated by more than one tomographic medical imaging modality for the purposes of diagnosis or therapy planning. It is not sufficient to consider soft tissue anatomy (provided by MR – Magnetic Resonance), bones morphology (CT – Computed Tomography) or functional information (SPECT or PET – Single Photon Emission or Positron Emission Tomography) in separate 3-D data sets. To exploit the benefit of their unique clinical information, it is useful to fuse them and visualize the complex information in single image. For the sake of different resolutions and objects orientation, to accomplish this complex image, volume registration is used to transform the data sets into a common coordinate frame.

A variety of approaches to the volume registration problem has been published until now. Good surveys were given by [Brown92] and [Maint98]. In order to make the physicians' work easier, attention is paid to fully-automatic methods for volume registration especially. There are two main approaches to this problem.

The first group represents feature-based methods which rely on pre-segmentation of specific features[1] or markers[2] in data sets and the matching of these features. However, automatic pre-segmentation of the features is a difficult task that can be solved successfully only if the features are well-defined. This is valid, for example, if artificial markers are firmly fixed with regard to the patient's anatomy, e.g. by implant markers, which is however very uncomfortable for a patient.

In order to avoid invasive intervention into the patient's body, a solid frame containing markers fixed firmly onto a patient can be used. Afterwards, a fully-automatic registration is done according to these markers[2]. The main advantages of such an approach are relatively low computational demands and high accuracy of the registration. However, the limitation represents the necessity of using an additional equipment – in this case the frame with markers.

The second group of methods is often called voxel-based[3], since they use directly the gray-level information carried by the voxels without segmentation of features. Therefore, these methods are more general and straightforward to apply. Practically, these methods always pose a kind of an optimization problem: having a criterion of registration quality, one has to find its global optimum in a pre-defined parametric space of geometrical transformations. In this paper, the registration aligns 3-D data sets of the head by using rigid body transformations with six degrees of freedom (three translations and three rotations).

In the case of multi-modality data sets the criterion must cope with non-linear dependencies of intensities of voxel pairs. The most popular criteria used at present days are derived from the information-theoretic approach, namely mutual information[3], or statistics, e.g. an algorithm published by Woods et al.[4]. In this paper we investigate different methods of their implementation and compare them regarding their computational demands and their suitability for a global optimization procedure.

Some optimization procedures are also studied, since they differ by their capability to find the global optimum in a parametric space often hidden among local optima and by speed of their convergence to the global optimum. The best optimizer requires the lowest number of evaluations of the optimized function and is robust with respect to local minima.

The main advantage of the voxel-based methods is their generality with regard to data sets and the fact that no user interaction is required during the registration. This is paid especially by a higher computational complexity. The computationally most expensive part is the recomputation of large 3-D data sets during optimization. To beat this problem particularly multi-resolution strategies are incorporated. The

used multi-resolution approach speeds up the registration process dramatically without the loss of accuracy.

Another way to acceleration of the registration procedure is pre-segmentation of data sets in order to avoid information of void voxels (background) to be used during optimization. This pre-segmentation is done fully-automatically by thresholding before the registration process starts.

The last technique that speeds up calculations is an innovative method of volume resampling. Commonly, if a volume data set is re-calculated according to a geometrical transformation, the position of every new voxel is computed by using a general 3D transformation matrix. This requires a lot of time-consuming floating point calculations. The presented method hinges on computations of only four such voxels. Then incremental vectors along three axis of a volume are computed and the new volume is calculated only by summation of these vectors. Moreover, during the resampling the realigned volume is traversed using integer arithmetic allowing to apply fast bit processor instructions.

The registration was tested on standard multi-modality data sets provided by Vanderbilt university, USA[5].

2. Data

To show the functionality of the developed registration method, standard inter-subject data sets of two modalities – CT and MR – are used. These data sets are provided in the framework of "The Retrospective Registration Evaluation Project" hold by J. Michael Fitzpatrick from Vanderbilt University, Nashville, TN, USA[5]. The project is designed to compare retrospective CT-MR and PET-MR registration techniques. It gives possibility to use an FTP database to allow the downloading of multimodal volumes on which registrations can be performed.

In this paper we focus on CT-MR registration. CT data sets (Figure 1) have resolution of 512 x 512 x 28 voxels, every voxel having the size 0.653595 x 0.653595 x 4.00 mm^3. MR data sets (Figure 2) are of 256 x 256 x 26 resolution with 1.25 x 1.25 x 4.00 mm^3 voxel size. Every voxel is expressed by a signed integer digit (32 bits). Please, note that although both the figures describe a slice through the same head, dependencies in gray-level information carried by the slices are non-linear; for example, white bones in CT correspond to black bones in MR.

3. Methods and results

The voxel-based registration methods consist of two main parts: of a criterion of registration quality – it can be called „similarity measure", since, in fact, it measures the similarity of two data sets – and of an optimization strategy that searches for the global optimum of the similarity measure in a predefined parametric space. The following sections give a detailed explanation of these two parts together with some remarks to their implementation.

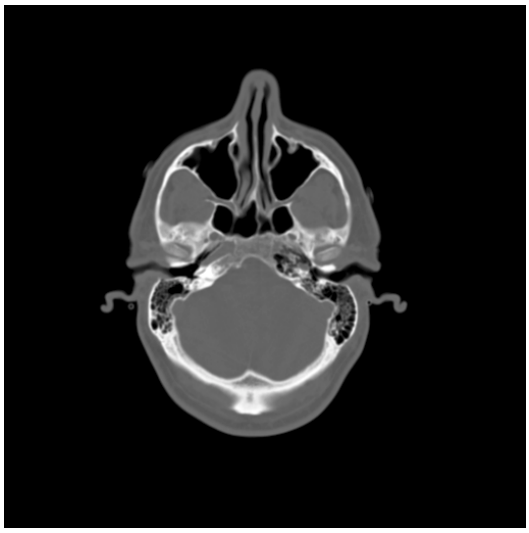

Figure 1: *Example of CT slice.*

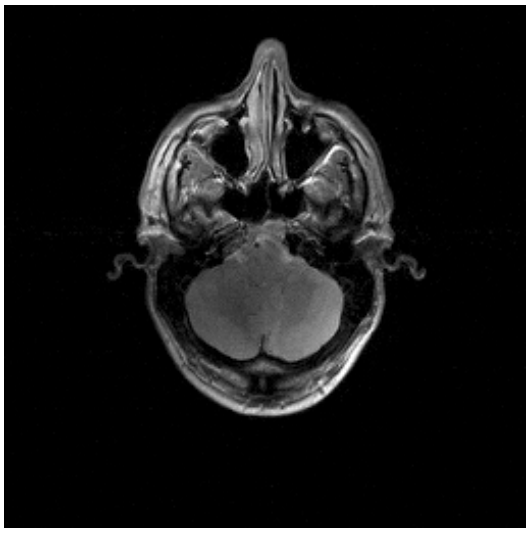

Figure 2: *Example of MR slice.*

3.1. Similarity measures

The most popular similarity measures used in medical volume registration are the ones derived from the information-theoretic approach or from statistics. The reason is that these criteria are able to handle nonlinear information relations between data sets. The most promising, namely an algorithm by Woods et al.[4] (WOODS), mutual information[3] (MI) and generalized mutual information[6] (GMI) will be discussed in more details. In case of mutual information two different algorithms of its evaluation were tested.

3.1.1. Woods's algorithm (WOODS)

Before the value of WOODS can be calculated, a 2D mutual histogram $g(a,b)$ according to Figure 3 is constructed – a and b represent gray values of the volumes u and v, respectively.

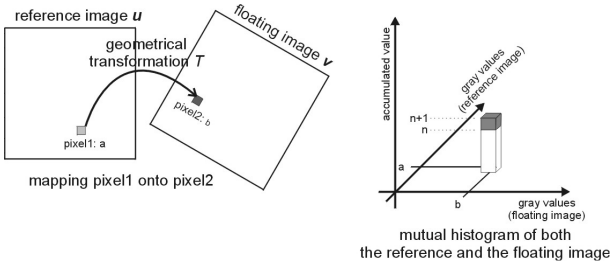

Figure 3: *Construction of the mutual histogram of two images (the same process is valid for 3D volumes).*

As a matter of fact, the value of WOODS represents a weighted sum of normalized standard deviations of gray values of voxels in the overlapped part of two volumes. The value of WOODS is obtained by the following formulas:

$$p^*(a) = \frac{\sum_b b\, g(a,b)}{\sum_b g(a,b)}$$

is the average value of voxels of volume *u* that correspond to the given voxel of volume *v*,

$$\sigma'(a) = \frac{1}{p^*(a)} \sqrt{\frac{\sum_b g(a,b)\left(b - p^*(a)\right)^2}{\sum_b g(a,b)}}$$

represents the normalized standard deviation of voxels of volume *u* corresponding to the given voxel of volume *v*,

$$V = \sum_{a,b} g(a,b)$$

stands for the mutual overlap of the volumes, and

$$WOODS = \sum_a [\sigma'(a) \frac{\sum_b g(a,b)}{V}]$$

is the resulting value.

3.1.2. Mutual information (MI)

Mutual information of two volumes *u* and *v* is defined in terms of entropy in the following way:

$$MI(u,v) = h(u) + h(v) - h(u,v),$$

where $h(.)$ is the Shannon entropy of a random variable and is defined as

$$h(x) = -\int p(x) \ln p(x) dx,$$

while the joint entropy of two random variables *x* and *y* is

$$h(x,y) = -\int p(x,y) \ln p(x,y) dxdy,$$

where *p* stands for probability of a random variable.

For practical evaluation mutual information can be re-written into probabilities calculated with the help of the mutual histogram (Figure 3). Then the value of mutual information is obtained according to Maes et al.[3]:

$$p_{uv}(x,y) = \frac{g(x,y)}{\sum_{a,b} g(a,b)},$$

$$p_u(x) = \sum_b p_{uv}(x,b),$$

$$p_v(y) = \sum_a p_{uv}(a,y),$$

$$MI = \sum_{a,b} p_{u,v}(a,b) \log_2 \frac{p_{uv}(a,b)}{p_u(a) p_v(b)}.$$

According to Fraser[7], in case of small data sets, the mutual histogram becomes a sparse matrix and MI is undervaluated. Therefore, he proposed a recursive algorithm that splits the histogram into small sub-areas having approximately the same number of incremental contributions, and the value of MI is computed through weighted evaluations of these sub-areas.

Fraser's algorithm was optimized by Weeks[8]. For fast calculation of MI of small data sets he applied a method based on sorting 2D arrays.

3.1.3. Generalized mutual information (GMI)

GMI is defined similarly to MI, but the Shannon entropies are replaced by the Renyi entropies[6] of the second order. According to the theory, this makes GMI more general and robust when compared with MI.

$$GMI(u,v) = h^{(2)}(u) + h^{(2)}(v) - h^{(2)}(u,v),$$

where

$$h^{(2)}(x) = -\int p^2(x) dx,$$

$$h^{(2)}(x,y) = -\int p^2(x,y) dxdy.$$

Practical implementation of GMI, like Weeks's implementation of MI, is based on sorting 2D arrays[6].

The above criteria have been tested with regard to their properties like smoothness, robustness, behavior in the vicinity of their global extreme and computational demand. The tests were accomplished by shifting two similar but not identical biomedical 3D images in the vicinity of their known registered position along *x* and *y* axes, i.e. in the vicinity of the global extreme of a similarity measure. The global extreme of the measure should be well-expressed in order to be easily localized in a parametric space by an optimization strategy. Moreover, it should have a smooth shape not disturbed by local extremes in which the optimization process could be undesirably trapped.

The quality of the measures in the vicinity of the global extreme is characterized by a parameter that we named AFA (Area of Function Attraction). It evaluates the range of convergence of a measure (expressed in voxels) to its global extreme. AFA counts the number of voxels from which the

global extreme is reached by applying a direct gradient method, i.e. downhill climbing according to a discrete gradient computed in every point of the parametric space. The higher the AFA, the better expressed and smoother the global extreme of the criterion.

The characteristic shapes of global extremes of the measures depicted in 2D plots are shown in Figures 4-7. The descriptions of these plots are accompanied by their corresponding AFA values. WOODS (Figure 4) has a sharp global extreme and, therefore, AFA is low. Generalized mutual information (Figure 7) has the value of AFA higher. MI according to Fraser & Weeks (Figure 6) has a sharp global extreme that is, moreover, masked by local ones. Hence, its AFA is low. MI computed according to Maes (Figure 5) has its global extreme well-expressed, broad and smooth and, thus, the value of AFA is the highest from the collection of the tested similarity measures.

The next test focuses on computational demands of the criteria. From the point of view of fast optimization the calculation of one value of the measure should be as fast as possible.

As mentioned above both MI according to Fraser & Weeks and GMI are computed by sorting 2D arrays which represent the input volumes. In other words, the computational time depends on their size, which is disadvantageous especially in case of large volumes. The computation times of one value of the criteria are shown in Table 1 (for simplicity for 2D case only). From the table follows that MI (Fraser & Weeks) is slightly faster than GMI, but the computational time of both the criteria is practically exponentially dependent on the size of evaluated data sets.

Image size	*MI (Fraser & Weeks)*	*GMI*
128 x 128	0,091 [s]	0,317 [s]
256 x 256	0,475 [s]	1,130 [s]
512 x 512	3,118 [s]	4,451 [s]
1024 x 1024	16,481 [s]	18,319 [s]

Table 1: *Times of the criteria computation for 2D images of different sizes (Pentium III, 600 MHz, 512 MB RAM).*

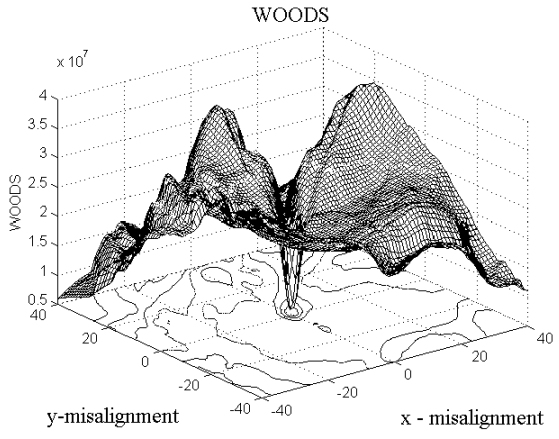

Figure 4: *WOODS, AFA = 390.*

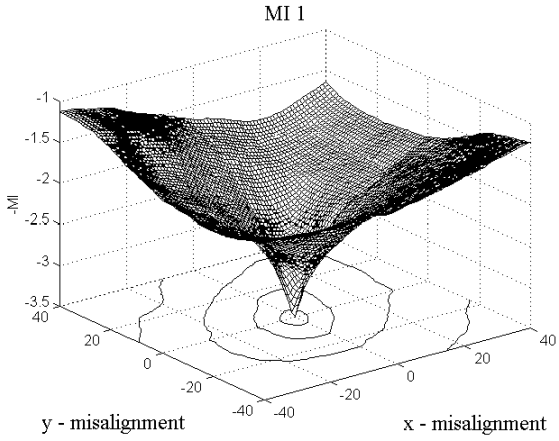

Figure 5: *MI (Maes), AFA = 6233.*

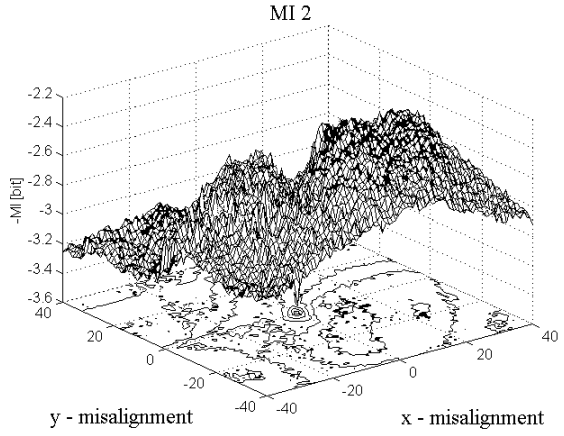

Figure 6: *MI (Fraser & Weeks), AFA 250.*

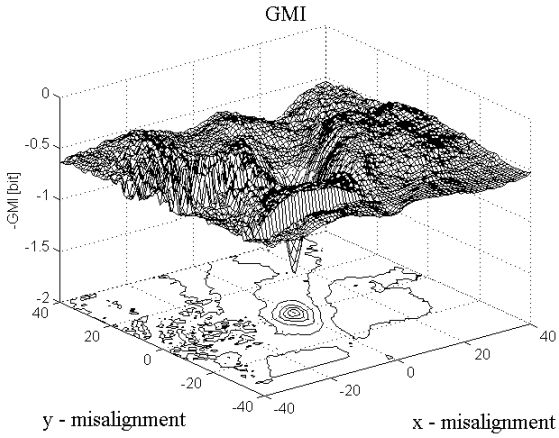

Figure 7: *GMI, AFA = 868.*

WOODS algorithm and MI according to Maes are calculated by a normalization of the 2D histogram. This means that after the histogram is filled in by values, the calculation of these criteria is independent of the size of the volumes. However, the computation demands depend on the size of the histogram, i.e. the number of histogram bins. These demands are illustrated in Table 2. It can be seen that MI (Maes) is faster than WOODS, and by applying lower number of histogram bins (e.g. 128) one can save further the computational time (e.g. about three times with respect to the full number of histogram bins, i.e. 256).

Histogram size	*WOODS*	*MI (Maes)*
64 x 64	0,019 [s]	0,012 [s]
128 x 128	0,031 [s]	0,021 [s]
256 x 256	0,134 [s]	0,062 [s]

Table 2: *Times of the criteria computation for histograms of different sizes (Pentium III, 600 MHz, 512 MB RAM).*

Considering the time requirements the criteria based on 2D histogram are more suitable for volume registration than the criteria based on sorting 2D arrays. From the histogram-based criteria MI according to Maes is the optimal choice, since it has a clear expressed global extreme. Therefore, it is easier to find it in a parametric space when compared with the extreme of WOODS (see Table 4). In order to preserve low computation demands it is advantageous for MI (Maes) calculation to apply the histogram having a size of about 150 x 150. Practical experiments confirm that this restriction does not decrease the accuracy of registration (see below).

3.2. Optimization strategies

An optimal optimization strategy should converge to the global extreme of an optimized function. This means that it should be robust regarding the presence of local extremes in a parametric space. Moreover, it should be fast, i.e. it should require only a small number of evaluations of the optimized function during the optimization process.

In this paper a set of optimization strategies including genetic algorithm[9], Powel's method[10], downhill simplex method (amoeba)[10] and adaptive simulated annealing[11] (ASA) has been tested. Table 3 summarizes briefly the results of the practical experiments.

genetic algorithm	*amoeba*	*Powell's method*	*ASA*
slow, possible convergences to local extremes	fast, frequent convergences to local extremes	fast, frequent convergences to local extremes	fast, possible convergences to local extremes

Table 3: *Behavior of different optimization methods.*

The genetic algorithm is a relatively robust strategy, however, its convergence to the global extreme is slow and it requires many evaluations of the optimized function to reach the extreme. Amoeba and Powell's method are faster optimizers, i.e. they require less evaluations of the optimized function when compared with the genetic algorithm, but they frequently terminate in local extremes. ASA is fast too and is more robust, i.e. it finds the global extreme with higher probability than amoeba or Powell's method, but still it converges from time to time to local extremes.

In order to show their effectiveness, amoeba, Powell's method and ASA were implemented in a stochastic manner. It means that every optimizer was multiply restarted from randomly selected positions of its starting point in a parametric space.

The stochastic implementation of the optimizers was evaluated by registration of identical volumes and by counting the number of successful registration results of all restarts (30 in this concrete test). Relative preciseness of all the strategies was set to 1.0E-7, i.e. the strategy terminated if the difference of the two last values of the applied measure is smaller than this number. Results are shown in Table 4 in percentages of successful results of all restarts. In the brackets relative numbers of evaluations of an optimized function during the optimization related to the value of stochastic ASA are given, e.g. stochastic Powell's method is by factor 1,60 (for MI) slower than stochastic ASA.

In order to demonstrate the importance of the shape of the global optimum of criteria, results of optimization of both WOODS and MI (Maes) are presented. Percentages confirm higher probability of finding the global extreme of MI (Maes) than of WOODS (see comments about AFA above).

	stochastic amoeba	*stochastic Powell's method*	*stochastic ASA*
MI (Maes)	~ 41% (0,73)	~ 24% (1,60)	**~ 70%** (1,00)
WOODS	~ 7% (0,55)	~ 13% (1,39)	**~ 54%** (1,00)

Table 4: *Effectiveness of stochastic optimizers (in percentages) applied to the histogram-based criteria (see text).*

Table 4 illustrates that the most suitable optimizer in our test is stochastic ASA – it is able to find the global extremes of the given criteria with the highest probabilities, 70% or 54%, respectively. Therefore, according to these results, we apply ASA to optimization of MI (Maes).

In practice it turned out that one start of the optimization strategy is sufficient, since objects in medical data sets have approximately the same position (in the middle). But the above mentioned experiment with the stochastic implementation of the optimizers demonstrates well the suitability of different optimization strategies for volume registration.

3.3. Remarks to the implementation

Medical volume data sets consist of a large number of voxels. During registration the main portion of computational time is consumed by the resampling of voxels of one volume with respect to the second volume according to actual geometrical transformation for which the criterion is evaluated. In order to lower the portion of voxels to be resampled, we eliminate the information void background of the studied object. The

processed subvolume is determined by thresholding prior to volume registration.

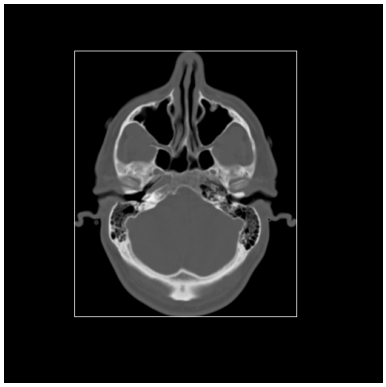

Figure 8: *The white frame shows a bounding box defining a subvolume that contains the entire object.*

This approach is illustrated in Figure 8. The white frame (bounding box) encloses the object and the voxels inside this frame represent, in this case, only 41% of the whole volume voxels that are used for the registration.

To diminish further the computational load, the registration is computed by using a low-resolution approach[12]. This means that not all voxels of the subvolume are used, but only a systematically selected subset. The subset is constructed by sub-sampling the volume with integral sampling factors f_x, f_y and f_z along the x, y and z coordinate axes using the nearest neighbor interpolation. This approach preserves geometric consistency of objects and ensures that each voxel in the volume affects the same histogram bins at all resolution levels, therefore, the optimum of MI is likely to be the same at all levels. Sub-sampling results in an acceleration by a factor of $F = f_x \cdot f_y \cdot f_z$.

sub-sampling factors (f_x ,f_y ,f_z)	$\lvert\Delta x\rvert$ [mm]	$\lvert\Delta y\rvert$ [mm]	$\lvert\Delta z\rvert$ [mm]	$\lvert\Delta\alpha\rvert$ [°]	$\lvert\Delta\beta\rvert$ [°]	$\lvert\Delta\chi\rvert$ [°]	*t* [sec]
1, 1, 1	0.00	0.00	0.00	0.00	0.00	0.00	6834.1
2, 2, 1	0.00	0.41	0.92	1.68	0.20	0.01	1528.8
3, 3, 1	0.01	0.35	1.51	1.64	0.15	0.05	713.2
4, 4, 1	0.01	0.18	0.01	0.05	0.04	0.08	421.9
5, 5, 1	0.08	0.38	1.43	1.68	0.30	0.04	278.0
6, 6, 1	0.04	0.18	1.50	1.62	0.42	0.08	206.5
8, 8, 1	0.02	0.02	0.05	0.03	0.02	0.28	134.8
10, 10, 1	0.11	0.49	1.56	1.53	0.32	0.31	90.8
12, 12, 1	0.11	0.04	1.83	1.42	0.12	0.28	67.9
16, 16, 1	0.08	0.30	1.32	1.58	1.01	0.10	48.3

Table 5: *Registration errors (related to the full resolution registration, i.e. $f_x=f_y=f_z=1$) and the computational times for the decreasing of resolution of multimodal volumes (CT- original resolution 512 x 512 x 28, MR – original resolution 256 x 256 x 26) to be registered (other registration parameters: histogram bins=64, ASA preciseness=1.0E-9).*

histogram bins	$\lvert\Delta x\rvert$ [mm]	$\lvert\Delta y\rvert$ [mm]	$\lvert\Delta z\rvert$ [mm]	$\lvert\Delta\alpha\rvert$ [°]	$\lvert\Delta\beta\rvert$ [°]	$\lvert\Delta\chi\rvert$ [°]	*t* [sec]
256	0.00	0.00	0.00	0.00	0.00	0.00	300.9
224	0.05	0.25	0.41	0.85	0.32	0.12	283.5
192	0.02	0.03	0.01	0.01	0.13	0.03	238.4
160	0.17	0.05	0.38	0.26	0.53	0.33	190.6
128	0.06	0.02	0.07	0.09	0.15	0.06	175.9
96	0.04	0.04	0.03	0.09	0.15	0.04	140.6
64	0.18	0.14	0.42	0.31	0.87	0.13	126.7
32	0.05	0.15	0.08	0.35	0.13	0.24	119.6

Table 6: *Registration errors (related to the full number of histogram bins, i.e. 256) and the computational times for the decreasing of number of histogram bins used for MI (Maes) computation (other registration parameters: sub-sampling factors=8,8,1; ASA preciseness=1.0E-9).*

ASA preciseness	$\lvert\Delta x\rvert$ [mm]	$\lvert\Delta y\rvert$ [mm]	$\lvert\Delta z\rvert$ [mm]	$\lvert\Delta\alpha\rvert$ [°]	$\lvert\Delta\beta\rvert$ [°]	$\lvert\Delta\chi\rvert$ [°]	*t* [sec]	*n. c. e.*
1,0E-10	0.00	0.00	0.00	0.00	0.00	0.00	228.7	6484
1,0E-9	0.21	0.06	0.55	0.27	0.52	0.17	126.3	3583
1,0E-8	0.16	0.02	0.46	0.23	0.44	0.17	62.9	1747
1,0E-7	0.39	0.39	0.27	1.47	1.06	0.29	29.1	822
1,0E-6	0.80	1.08	0.93	1.47	0.27	0.23	13.3	368
1,0E-5	6.22	6.30	11.13	21.2	22.5	16.01	6.0	169

Table 7: *Registration errors (related to ASA preciseness=1.0E-10), the computational times and numbers of criterion evaluations during optimization (n. c. e.) for the decreasing of preciseness of ASA optimization (other registration parameters: sub-sampling factors=8,8,1; histogram bins=64).*

Generally, it is sufficient to apply low-resolution registration only. This means that the registration is found for lower resolution only, and its result is applied directly to the full-resolution volumes. The practical comment about the implementation of the sub-sampling factors is that no low-resolution versions of the original volume data sets are created, but the resampling is done "on-fly". In other words, during evaluation of volume similarity voxels belonging to the sub-grid defined by the sub-sampling factors are taken directly from the first full-resolution volume and their counterparts are found in the second full-resolution volume.

As shown in Table 5 the accuracy of lower resolution registrations is acceptable even for high sub-sampling factors used and the process is faster. If exact registration is required, a two-level pyramidal hierarchy of registration can be applied. In this hierarchy we start at higher level of the pyramid (i.e. with low resolution). At the second level the number of voxels is increased to higher resolution (not necessarily to the full resolution).

Results in Table 5 were obtained for registration of the pair of multimodal data sets (CT, MR) as described in Section 2. The only altered registration parameters were the sub-sampling factors. The absolute valued errors of registrations are related to the results of the full resolution registration. The investigated parametric space was ±50 mm for translations along all coordinate axes (x, y, z) and ±30° for rotations (α, β, χ) around theses axes. Table 5 exemplifies significant acceleration of the registration process, while the sub-voxel registration accuracy (i.e. the translation errors are smaller than the voxel dimensions) is preserved even for high sub-sampling factors.

Another approach that speeds up the registration process significantly is an efficient implementation of volume resampling. Usually, during volume resampling according to the geometrical transformation every new voxel is calculated by using a general 4 x 4 transformation matrix T:

$$v(x,y,z) = T(u(x,y,z)).$$

This requires a lot of time-consuming floating point processor operations, especially multiplications.

To avoid this time complexity the following approach has been used: having a transformation matrix T, four voxels lying at corners of the original volume ([0,0,0], [Xmax,0,0], [0,Ymax,0], [0,0,Zmax]) are transformed into their new positions. With the help of these positions incremental vectors along the coordinate axes are determined. Knowing the position of the origin of coordinate system of the resulting volume, i.e. T([0,0,0]), the new volume is resampled by using the incremental vectors for stepping with the help of trilinear interpolation.

When using floating point arithmetic, this method speeds up the registration by factor about 1,10 only. To achieve more progressive acceleration, the coordinate system is scaled by a factor of 2^{16}, in order to be able to use integer arithmetic instead. This transformation allows to traverse the volume by using additions and bit shift operations only.

Table 8 illustrates an example of average volume resampling times for the registration of the same pair of low-resolution volumes by using either standard or the described fast implementation of the volume resampling.

standard implementation	0.1389 [sec]
fast implementation	0.0349 [sec]

Table 8: *Comparison of average times of volume resampling during registration in case of standard implementation and the presented fast (integer) implementation of volume resampling (the speed-up factor=3,98).*

As mentioned in Section 3.1. the registration can be accelerated by lowering the number of histogram bins too. The corresponding results are shown in Table 6, where the errors of registration computed with lower numbers of bins are related to the result obtained for the maximal number of bins (256). The sub-voxel registration accuracy is kept for small histogram sizes too.

Table 7 shows registration errors and the computational times in case of lowering the preciseness of applied optimization strategy (ASA). Another parameter in the table is the number of criterion evaluations (n. c. e.) during registration. From the table follows that if the preciseness is smaller than 1.0E-7, sub-voxel accuracy is not obtained (for 1.0E-6) or the result can be completely wrong (for 1.0E-5). In practice it is not advantageous to speed-up the registration process by lowering the ASA preciseness. On the contrary, it is better to use even higher values (1.0E-8, 1.0E-9) which increase probability to reach the global extreme of the criterion even if the high sub-sampling factors and the small number of histogram bins are applied.

In order to demonstrate the resulting speed-up factor, first (I) the registration of the pair of data sets (CT, MR) was performed with the full resolution volumes, 256 histogram bins and standard implementation of volume resampling. Afterwards (II), the sub-sampling factors f_x, f_y, f_z were set to 8, 8, 1, number of histogram bins was decreased to 96 and fast implementation of volume resampling was used. The resulting times are in Table 9, while the differences in geometrical transformation parameters of both registrations was in sub-voxel range.

I	28742.2 [sec]
II	148.3 [sec]

Table 9: *Comparison of times of registration of full resolution volumes (I) and low-resolution volumes (II), see text for detailed explanation, the resulting sped-up factor=193,81 (Pentium III, 600 MHz, 512 MB RAM).*

In practice it is very useful to apply different registration parameters for different tasks. To obtain the registration quickly (for a glance), one can use high sub-sampling factors and low number of histogram bins or, on the contrary, if he/she wants to have a precise result (e.g. for surgery planning) he will use low sub-sampling factors and high number of histogram bins.

Figures 9 and 10 exemplify fusion images of some registration results.

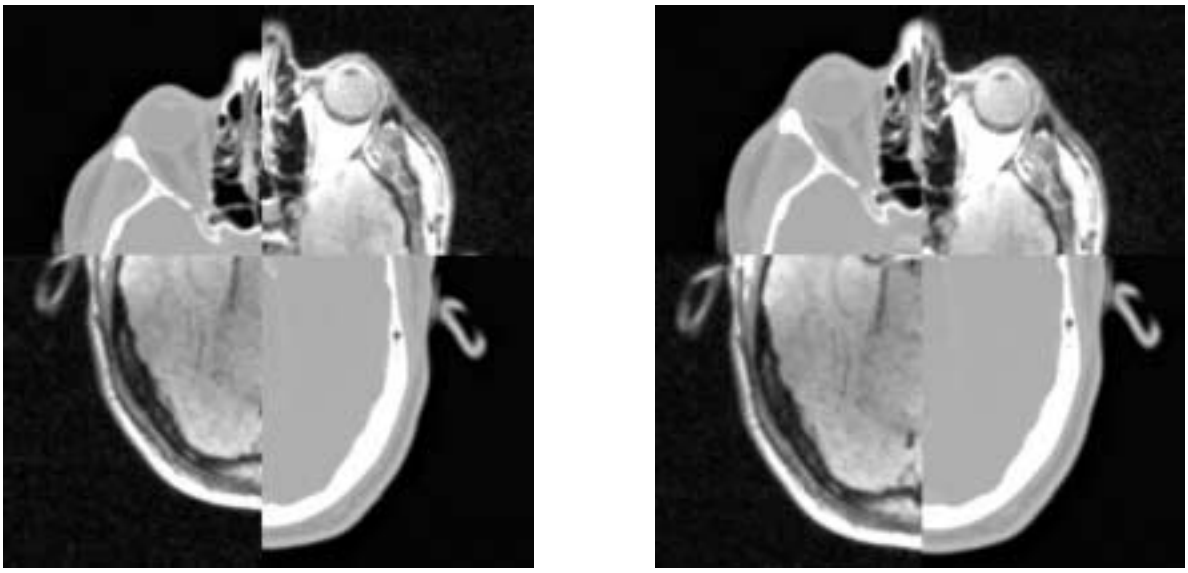

Figure 9: *2D examples of axial CT-MR fusion images before (the left image) and after registration (the right image); (CT - the upper left and the lower right parts of the images).*

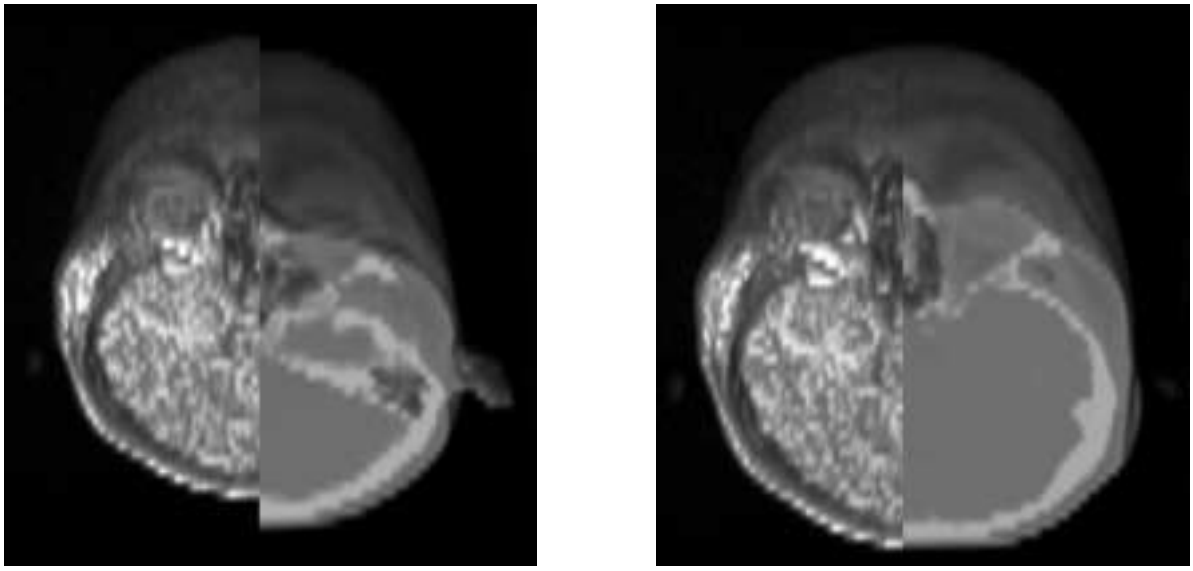

Figure 10: *3D examples of CT-MR fusion images before (the left image) and after registration (the right image); (CT - the right parts of the images).*

4. Conclusion

The fast and robust volume registration procedure is presented. Its performance enables it to be applied on common PC machines, which gives opportunity to be implemented in PC-based medical visualization systems and, thus, to be used in routine practice.

The absolute accuracy of the proposed registration methods will be evaluated in the framework of "The Retrospective Registration Evaluation Project"[5], and by using multimodal data sets provided by SIP Laboratory (University Department of Radiology, Innsbruck, Austria) where the data sets will be aligned by using external markers[2] as a "gold standard" and the results will be compared with results of the full-automatic registration method.

Acknowledgements

VRVis – Research Center for Virtual Reality und Visualization – is supported by the Austrian "K plus" research program, *http://www.vrvis.at*.

The figures 9 and 10 in this paper are courtesy of TIANI Medgraph GesmbH, Vienna, Austria, *http://www.tiani.com*.

The 3D images were provided as part of the project, "Evaluation of Retrospective Image Registration", National Institutes of Health, Project Number 1 R01 NS33926-01, Principal Investigator, J. Michael Fitzpatrick, Vanderbilt University, Nashville, TN, *http://cswww.vuse.vanderbilt.edu/~image/registration*.

References

1. Maurer, C. R., et al.: Registration of 3-D Images Using Weighted Geometrical Features. *IEEE Trans. Med. Imag.*, **15**(6):836–849, December 1996.
2. Čapek, M., et al.: "Multimodal Medical Registration Based on Spherical Markers", *Proc. of WSCG'2001, Pilsen, Czech Republic*, **1**: 17–24, February 2001.
3. Maes, F., Collignon, A., Vandermeulen, D., Marchal, G., Suetens, P.: Multimodality Image Registration by Maximization of Mutual Information. *IEEE Trans. Med. Imag.*, **16**(2):187–198, April 1997.
4. Woods, R. P., Mazziotta, J. C., Cherry, S. R.: MRI-PET Registration with Automated Algorithm. *Journal of Computer Assisted Tomography*, **17**(4):536–546, July/August 1993.
5. http://cswww.vuse.vanderbilt.edu/~image/registration/
6. Pompe, B., Heilfort, M.: On the Concept of the Generalized Mutual Information Function and Efficient Algorithms for Calculating it. http://ap01.physik.uni-greifswald.de/~pompe, February 1995.
7. Fraser, A. M.: Information and Entropy in Strange Attractors. *IEEE Trans. Inf. Theory*, **35**(2):245–262, March 1989.
8. http://chaos.ph.utexas.edu/~weeks/software/minfo.html
9. Parker, J. R.: *Algorithms for Image Processing and Computer Vision*. John Wiley & Sons, Inc., New York, pp. 357-386, 1997.
10. Press, W. H., et al.: *Numerical Recipes in C: the Art of Scientific Computing*. 2nd ed., Cambridge University Press, New York, 1992.
11. Ingber, L.: Simulated Annealing: Practice versus Theory. *Mathl. Comput. Modelling*, **18**(11):29–57, 1993.
12. Maes, F., Vandermeulen, D., Suetens, P.: Comparative evaluation of multiresolution optimization strategies for multimodality image registration by maximization of mutual information. *Medical Image Analysis*, **3**(4):373–386, 1999.